Mechanism of Carbene Formation from the Excited States of Diazirine and Diazomethane: An MC-SCF Study

Naoko Yamamoto,[§] Fernando Bernardi,[†] Andrea Bottoni,[†] Massimo Olivucci,*[,†] Michael A. Robb,*[,§] and Sarah Wilsey[§]

Contribution from the Dipartimento di Chimica "G. Ciamician" dell'Università di Bologna, Via Selmi 2, 40126 Bologna, Italy, and the Department of Chemistry, King's College, London, Strand, London WC2R 2LS, U.K.

Received June 14, 1993[⊕]

Abstract: Three radiationless decay pathways for the photochemical decomposition of diazirine and diazomethane have been characterized using the MC-SCF method with a 6-31G* basis. From diazirine, two almost barrierless paths exist on S_1. One leads, via a diradicaloid $^1D_{\sigma\pi}$ conical intersection at a bent, in-plane, diazomethane-like structure, to ground-state diazomethane; the other leads, via another $^1D_{\sigma\sigma}$ conical intersection at a ring-opened diazirine diradicaloid geometry, directly to $^1CH_2 + N_2$. The triplet pathway starts at a $^3\pi$–π^* diazirine minimum, passing over a 9 kcal mol^{-1} barrier to a ^3n–π^* $^3D_{\sigma\pi}$ bent diazomethane-like minimum from which the barrier to N_2 extrustion is 7 kcal mol^{-1}. In the absence of sensitizers, this triplet path can be entered from the singlet manifold via intersystem crossing at a point that has been characterized by finding the lowest energy point on the singlet–triplet crossing surface. This crossing point occurs at a geometry that is very similar to the transition state that occurs on the singlet path between diazirine and ground-state diazomethane. However, the efficiency of intersystem crossing (spin–orbit coupling) is predicted to be low. These data rationalize the temperature dependence of the fluorescence, the fact that diazomethanes and diazirines are observed as products of photolysis of diazirines and diazomethanes, respectively, the fact that there is $CH_2 + N_2$ formation from both diazirines and diazomethanes, and the fact that no triplet states seem to be involved in the reaction.

Introduction

The photolysis of diazirines (for recent work, see, for example, refs 1–7 and the discussion in the book of Michl[8]) produces an electronically excited n–π^* state which can, in principle, decay by at least four competitive pathways (illustrated in Scheme 1): (1) fluorescence, (2) intersystem crossing with the production of a triplet carbene, (3) formation of an excited-state diradical followed by internal conversion and production of singlet carbene with N_2 extrusion, and (4) adiabatic rearrangement and subsequent internal conversion to diazoalkane isomers. In addition, in substituted diazirines containing at least one α-H, it has been recently proposed[5] that an additional competitive process involving simultaneous (i.e., concerted) [1,2] H-shift and N_2 extrusion is possible.

While the intermolecular chemistry of CH_2 has a sound experimental and theoretical basis, the mechanism of its production via the photochemical extrusion of N_2 from diazirines and diazomethane remains the subject of debate. The photophysics and photochemistry of diazirine has been the subject of several recent experimental studies[1–7] with modern fluorescence equipment, and new detailed information about the mechanism of the photodecomposition is now available. However, the only theoretical basis for the rationalization of this information comes from the semiempirical work of Jug and co-workers[9] and the much earlier ab initio work of Devaquet,[10] carried out in 1978. Though there is considerable experimental information supporting the existence of all of the four decay pathways suggested above in various substituted diazirines, this experimental information has never been successfully rationalized from a mechanistic point of view. The object of our work is to document the possible reaction paths from the Franck–Condon region to final products and to rationalize the recent photophysical[1–6] experiments using the unsubstituted diazirine and diazomethane model systems.

Scheme 1

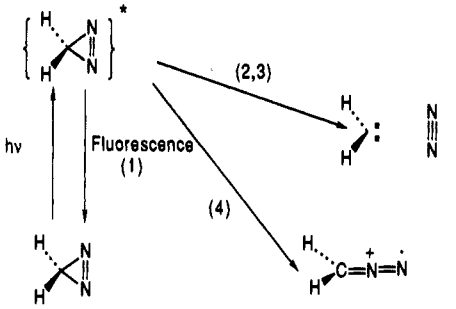

In discussing the various potential energy surfaces, we will always use fully optimized geometries and reaction paths (optimized via intrinsic reaction coordinate calculations) so that the results are independent of any specific choice of internal variables. However, from the outset, it is convenient to use some qualitative internal variables (shown in Scheme 2) that will provide a means for discussing our results in a general way. We are concerned with the potential energy surface that connects diazomethane (Scheme 2a, C_{2v}) and diazirine (Scheme 2c, C_{2v}) to three transient species: bent, in-plane diazomethane (Scheme

[§] King's College London.
[†] Università di Bologna.
[⊕] Abstract published in *Advance ACS Abstracts*, January 15, 1994.

(1) Seburg, R. A.; McMahon, R. J. *J. Am. Chem. Soc.* **1992**, *114*, 7183–7189.
(2) Ammann, J. F.; Subramanian, R.; Sheridan, R. S. *J. Am. Chem. Soc.* **1992**, *114*, 7592–7594.
(3) Chen, N.; Jones, M., Jr.; Platz, M. S. *J. Am. Chem. Soc.* **1991**, *113*, 4981–4992.
(4) Modarelli, D. A.; Platz, M. S. *J. Am. Chem. Soc.* **1991**, *113*, 8985–8986.
(5) Modarelli, D. A.; Morgan, S.; Platz, M. S. *J. Am. Chem. Soc.* **1992**, *114*, 7034–7041.
(6) Modarelli, D. A.; Platz, M. S. *J. Am. Chem. Soc.* **1993**, *115*, 470–475.
(7) O'Gara, J. E.; Dailey, W. P. *J. Am. Chem. Soc.* **1992**, *114*, 3581–3590.
(8) Michl, J.; Bonacic-Koutecky, V. *Electronic Aspects of Organic Photochemistry*; Wiley: New York, 1990.
(9) Müller-Rammers, P. L.; Jug, K. *J. Am. Chem. Soc.* **1985**, *107*, 7275–7284.
(10) Bigot, B.; Ponec, R.; Sevin, A.; Devaquet, A. *J. Am. Chem. Soc.* **1978**, *100*, 8575.

0002-7863/94/1516-2064$04.50/0

Scheme 2

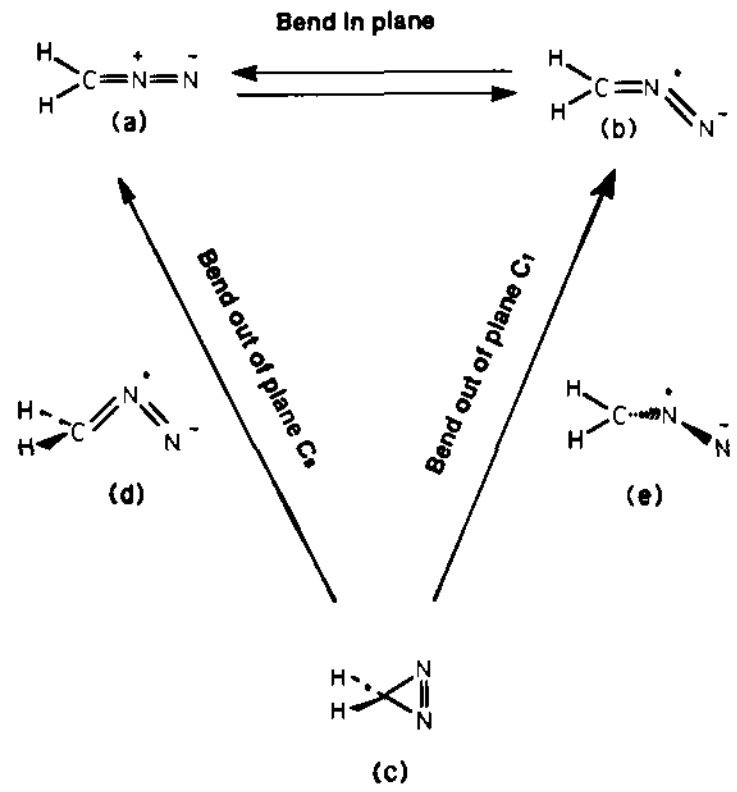

Chart 1

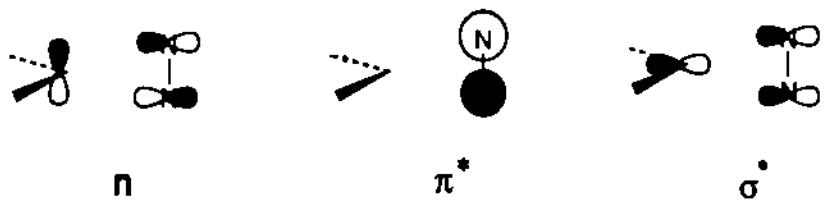

2b, C_s); bent, out-of-plane diazomethane (Scheme 2d, C_s); and twisted, bent, out-of-plane diazomethane (Scheme 2e, C_1). Thus, in addition to a coordinate involving fragmentation to N_2 and CH_2, we shall distinguish three other coordinates: (1) a bent in-plane (**bip**) coordinate that connects the structures of Scheme 2a and b, and retaining one of the reflection planes, (2) a bent, out-of-plane (bop-C_s) coordinate that connects the structures of Scheme 2a and c, retaining the other reflection plane, and (3) a bent, out of plane (**bop**-C_1) coordinate that connects the structures of Scheme 2b and c, where all the symmetry is lifted. We emphasize that these coordinates are introduced only to facilitate the discussion, and we define them only qualitatively via Scheme 2.

The mechanistic features of diazirine photochemistry will involve a discussion of many reaction paths on several potential energy surfaces. Thus, by way of introduction, it is useful to discuss the theoretical background in terms of a simple, qualitative valence bond (VB) model of the potential energy surfaces involved in the photochemistry and photophysics. The presentation of our own results will then be unified using this model.

The initial singlet state of diazirine is thought to result from an n-to-π^* excitation using the orbitals sketched in Chart 1 (where we have used the nomenclature coined originally by Devaquet[10] to label the orbitals). The n–π^* state can be represented in VB terms as shown in Chart 2a (the N_2 π-orbitals are shown separately). In this VB diagram, the orbitals that are spin-coupled are indicated by lines, doubly occupied atomic orbitals by pairs of arrows, and loosely coupled diradical pairs by single arrows. We give only a single example of each type of spin pairing. Clearly, simple adiabatic extrusion of N_2 from this state (Chart 2a) would lead diabatically to $^3CH_2$ and $^3\pi$–π^* N_2 or excited $^1CH_2$ and $^1\pi$–π^* N_2.

Along the **bop**-C_s coordinate, diazirine (Chart 2a) would become an open-chain σ–π diradical, which we shall denote as $^{1,3}D_{\sigma\pi}$. This $^{1,3}D_{\sigma\pi}$ diradical is essentially the n–π^* state of diazomethane (structure shown in Chart 2c). Alternatively, along a bop-C_1 coordinate, we reach a bent, in-plane diazomethane via a rather complicated deformation involving C–N–N bending and rotation

Chart 2

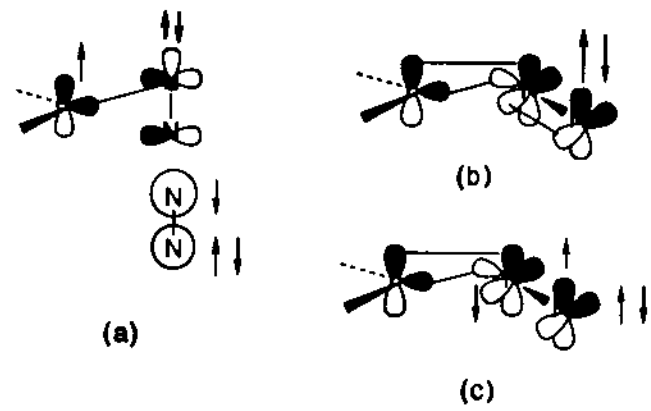

Chart 3

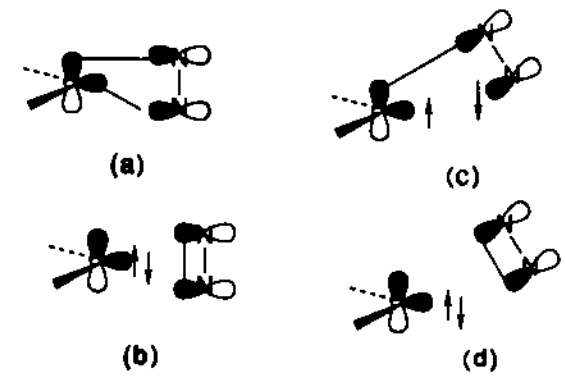

about the C–N bond. By spin-paring the CH_2 p^π orbital with the N_2 p^π orbital, the structure of Chart 2a would correlate directly with that of Chart 2b, the ground state of diazomethane.

It is often assumed that the photochemistry of diazirines involves the n–σ^* state.[9,10] The n–σ^* state can be thought of as a simple spin-recoupling of the ground-state configuration in VB language. Thus, the ground state of diazirine corresponds to the VB structure shown in Chart 3a while the n–σ^* state corresponds to the VB structure shown in Chart 3b. It is obvious that N_2 extrusion from the structure in Chart 3b would lead to ground-state N_2 and CH_2 diabatically from the n–σ^* state. Ring opening along a **bop**-C_s coordinate would lead to a $\sigma\sigma$ diradical, Chart 3c, which we shall denote as $^{1,3}D_{\sigma\sigma}$.

Theoretical methods provide the only technique for determining the behavior of the various excited-state potential energy surfaces. Both Devaquet et al.[10] and Jug et al.[9] have studied a **bop**-C_s coordinate and N_2 extrusion coordinate in some detail. They both suggest that $^{1,3}D_{\sigma\sigma}$ and $^{1,3}D_{\sigma\pi}$ structures are central to the understanding of the mechanism. However, neither study was able to characterize the surface crossings with a reliable method. In C_{2v} symmetry, the n–σ^* state and n–π^* state have different symmetry, and there must be a n–σ^*/n–π^* conical intersection, as pointed out by Jug.[9] Thus, for a direct photochemical pathway that starts on the n–π^* state and proceeds onto the n–σ^* state, the reaction path must "curve" (bop-C_1 path) so that the crossing becomes avoided and a transition state occurs. While Devaquet et al.[10] have studied N_2 extrusion along a **bip** coordinate, they have assumed a C–N–N angle of 110°. There is no theoretical information about the energy surface in a **bop**-C_1 versus N_2 extrusion subspace. In our calculations we make no assumptions about the symmetry of the reaction paths which have been determined via unconstrained transition-state search and intrinsic reaction coordinate (IRC) calculations.

We now briefly review the experimental background. Two different experimental strategies have been recently applied to study the photolysis of alkyldiazirines. The first is based on the photolysis of matrix-isolated diazirines and diazomethanes where the temperature of the matrix is held at 6–8 K.[1,2] The second method involves the use of laser flash photolysis (LFP) techniques to observe transient and trapped species at room temperature.[3-6] Previous experimental results can be found in refs 11–24 and will not be discussed here.

(11) Frey, M. H. *Adv. Photochem.* **1966**, *4*, 225.

McMahon and Seburg[1] have produced a rather complete study of the matrix isolation photolysis of 3-methyldiazirine (MD) and diazoethane (DE) where the irradiation conditions and the type of matrix (Ar, N_2, Xe) are varied in order to avoid matrix-dependent photochemistry. Photolysis of MD and of its trideuterio isotope, MD-d_3, in a CO-doped argon matrix leads to the formation of small amounts of ketenes as a result of ethylidene (i.e., carbene) trapping. The formation of a small amount of ketene from carbene and CO is consistent with the presence of a very fast ethylidene [1,2] H-shift which efficiently competes with CO trapping. This fast [1,2] H-shift should then be the only source of ethylene, which is the major detectable product of the reaction. MD photolysis in a $^{14}N_2$ matrix at 8 K produces ethylene and a trace of DE, indicative of MD-to-DE photoisomerization. Since irradiation of ^{14}N-DM in $^{15}N_2$ matrix at 8 K leads to no incorporation of ^{15}N in DE, the authors exclude DE formation by reaction of ethylidene with the N_2 matrix. This result is at variance with older data by Moore and Pimentel.[15]

The photolysis of DE and DE-d_3 in CO-doped argon matrix leads to the same conclusion reported for MD, since a small amount of ketene is detected in this case as well. In the case of the photolysis of DE in argon matrix, the authors also detected competitive formation of MD, which originates via photochemical isomerization of DE. In this case the authors were able to quantify the product ratio ethane:diazirine to be 10:1. In conclusion, matrix isolation experiments at 8 K support a straightforward mechanism where a transient carbene is the major intermediate in the production of alkenes from both diazirines and diazoalkanes. Two less efficient but detectable reactive channels lead to competitive formation of diazoalkanes and diazirines via photoisomerization of diazirines and diazoalkanes, respectively. The simultaneous formation of diazoalkanes and singlet carbenes has been also detected in matrix-isolated photolysis of differently substituted diazirines. For instance, Sheridan et al.[2] have detected dicyclopropylcarbene via IR spectroscopy in a 6 K N_2 matrix, which was confirmed via CO trapping. The second major product of the photolysis (334 nm, 28 h) detected was dicyclopropyldiazomethane, which produced the same dicyclopropylcarbene intermediate by broad-band irradiation above 340 nm.

Recent spectroscopic and LFP studies on alkyldiazirines photolysis have been carried out by Mondarelli, Platz, and co-workers.[3-6] The results of LFP studies on 3,3-dimethyldiazirine[5] and 3-methyldiazirine-d_4[6] indicates the formation of short-lived singlet carbenes which can be trapped with pyridine. Under the same conditions, the presence of diazoalkane isomers that are observed during the photolysis of other bulkier diazirines such as adamantyldiazirine could not be detected by LFP.[6] Mondarelli, Platz, and co-workers conclude that photochemical isomerization to diazoalkanes must be a low-yield process, in agreement with the matrix isolation data seen above. The same workers also report a temperature dependence of the fluorescence intensity study of 3,3-dialkyldiazirines.[5] These data show a decrease in intensity as the temperature is increased. This loss in fluorescence intensity is associated with an activation barrier that ranges from 0.02 to 1.5 kcal mol^{-1}. These data thus provide evidence of very efficient decay paths for the photodecomposition of diazirines after passage over a very small barrier. A similar study on the dependence of the fluorescence intensity by isotopic labeling has lead to the formulation of a new reaction mechanism for diazirine photodecomposition.[5] According to the data, 3,3-dimethyldiazirine-d_6 shows a fluorescence intensity about 50% greater than that of 3,3-dimethyldiazirine. This has been taken as evidence for H migration in the excited state of diazirines with at least one α-H. The authors indicate that, according to their data, about 60% of propene + N_2 production is due to this hydrogen shift mechanism, which would involve concerted N_2 extrusion without production of a carbene intermediate.

The role of triplet states in diazirine photochemistry has also been investigated. Laser flash photolysis of 3-methyldiazirine in pentane saturated with oxygen carried out recently by Mondarelli et al.[6] failed to produce a detectable quantity of carbonyl oxide, indicating the absence of the triplet carbene (i.e., ethylidene) intermediate. They concluded that the rate of intersystem crossing (ISC) in ethylidene is lower than the rate of isomerization to ethylene. The same authors found no compelling evidence for intersystem crossing ($S_1 \rightarrow T_1$) in the excited state of 3-methyldiazirine[6] and 3,3-dimethyldiazirine[5] at room temperature and could not detect triplet–triplet transient absorption of T_1 upon laser flash photolysis of 3,3-dimethyldiazirine in pentane. Thus, they concluded that the triplet state of dimethyldiazirine either is not formed on direct photolysis of dimethyldiazirine in solution or has an exceptionally short lifetime.

McMahon and Seburg[1] have also investigated the possible involvement of ISC in the matrix-isolated photochemistry of 3-methydiazirine and diazoethane. These products were photolyzed in Xe matrix in the hopes of increasing ISC rate by the heavy atom effect. However, ESR spectra failed to detect any triplet signal. The failure to detect triplet carbene, which might be generated via ISC from nascent singlet carbene, has also been tested by the same authors. The carbene-to-alkene [1,2] H-shift was slowed via deuterium substitution in both 3-methyldiazirine and diazoethane in order to make the ISC more competitive. Similarly, in this case, no triplet signals were detected.

In summary, from the experimental results, diazirine photochemistry and photophysics is dominated by one or more efficient radiationless decay paths, as indicated by the temperature dependence of the fluorescence. These decay paths could involve the direct formation of singlet carbene with N_2 extrusion or rearrangement to diazoalkane isomers. Two similar photochemical processes also appear to occur starting from diazoalkanes. Decay of photoexcited reactant via intersystem crossing to T_1 to produce triplet carbenes seems less probable. A further photochemically relevant decay mechanism could involve concerted [1,2] H-shift and N_2 extrusion. While this mechanism would deserve theoretical investigation, it is limited to diazirines bearing at least one α-H. In addition, the efficiency of the possible reaction paths will also be affected by substitution. However, we will limit our discussion to the photoreactivity which can be assigned to the diazirine and diazomethane moieties alone.

Computational Details

All CAS-SCF computations have been performed using the MC-SCF program distributed in Gaussian 92[25] using a 6-31G* basis. For all calculations, the active space chosen is unambiguous: six electrons, distributed in four active orbitals from N_2 plus the pσ and pπ orbitals of the CH_2 moiety. Location of the excited-state minima and transition structures and mapping of the intrinsic reaction coordinates have been carried out by using the methods available in the Gaussian package.

(12) Evans, W. B. L. Ph.D. Thesis, University of Southampton, UK, 1966.
(13) Bradley, G. F. Ph.D. Thesis, University of Southampton, UK, 1967.
(14) Amrich, M. J.; Bell, J. A. *J. Am. Chem. Soc.* **1964**, *86*, 292.
(15) Moore, C. B.; Pimentel, G. C. *J. Chem. Phys.* **1964**, *41*, 3504.
(16) Paulett, G. S.; Ettinger, R. *J. Chem. Phys.* **1963**, *39*, 82. Paulett, G. S.; Ettinger, R. *J. Chem. Phys.* **1963**, *39*, 3534.
(17) Paulett, G. S.; Ettinger, R. *J. Chem. Phys.* **1964**, *41*, 2557.
(18) Frey, H. M.; Penny, D. E. *J. Chem. Soc., Farad. Trans. 1* **1977**, *73*, 2010.
(19) Liu, M. T. H. *Chem. Soc. Rev.* **1982**, *11*, 136.
(20) Avila, M. J.; Becerra, R.; Figuera, J. M.; Rodriguez, J. C.; Tobar, A. *J. Phys. Chem.* **1985**, *89*, 5489.
(21) Kirmise, W.; Buschoff, M. *Angew. Chem., Int. Ed. Engl.* **1956**, *4*, 692.
(22) Frey, H. M.; Scaplehorn, W. *J. Chem. Soc. A* **1966**, 968.
(23) Chang, K. T.; Shechter, H. *J. Am. Chem. Soc.* **1979**, *101*, 5082.
(24) Newman-Evans, R. H.; Simon, R. J.; Carpenter, B. K. *J. Org. Chem.* **1990**, *55*, 695.
(25) Frisch, M. J.; Trucks, G. W.; Head-Gordon, M.; Gill, P. M. W.; Wong, M. W.; Foresman, J. B.; Johnson, B. G.; Schlegel, H. B.; Robb, M. A.; Replogle, E. S.; Gomperts, R.; Andres, J. L.; Raghavachari, K.; Binkley, J. S.; Gonzalez, C.; Martin, R. L.; Fox, D. J.; Defrees, D. J.; Baker, J.; Stewart, J. J. P.; Pople, J. A. *Gaussian 92*, Revision B; Gaussian Inc.: Pittsburgh, PA, 1992.

Table 1. Ground- and Excited-State Structures and Energetics for the Potential Energy Surfaces of Diazirine/Diazomethane

geometry	state	energy, E_h	relative energy (kcal mol^{-1})
$N_2 + {}^1CH_2$ ($^1A_1$)		−147.9284	0
$N_2 + {}^1CH_2$ ($^1B_1$)		−147.8811	29.7
ground-state diazirine (Figure 1a)	S_0	−147.9404	−7.5
	^1n–π^*	−147.7545	109.1
	$^3\pi$–π^*	−147.7708	
	^3n–π^*	−147.7352	
ground-state diazomethane (Figure 1b)	S_0	−147.9638	−22.2
	^1n–π^*	−147.7941	84.3
	^3n–π^*	−147.8047	
diazirine S_1 minimum (Figure 1c)	^1n–π^*	−147.7656	102.2
diazirine–diazomethane S_1 transition state (Figure 1d)	^1n–π^*	−147.7651	102.5
diazomethane S_0/S_1 $^1D_{\sigma\pi}$ conical intersection (Figure 1e)	^1n–π^*/S_0	−147.871	36.1
$^1D_{\sigma\sigma}$ conical intersection, Chart 2c (Figure 1f)	^1n–σ^*/S_0	−147.832	60.4
diradical–diazomethane transition state (Figure 1g)	^1n–$\sigma^*/^1n$–π^*	−147.8263	64.1
diazirine ^1n–$\sigma^*/^1n$–π^* conical intersection (Figure 1h)	^1n–$\sigma^*/^1n$–π^*	−147.746	114.7
$N_2 + {}^3CH_2$		−147.9515	0
diazirine T_2/S_1 intersection (Figure 6a)	^1n–$\pi^*/^3n$–π^*	−147.771	113.5
diazirine T_1 minimum (Figure 6b)	$^3\pi$–π^*	−147.8077	90.23
diazomethane $^3D_{\sigma\pi}$ minimum (Figure 6c)	^3n–π^*	−147.9008	31.8
$^3D_{\sigma\pi}$ diazomethane–diazomethane CN rotational transition state (Figure 6d)	^3n–σ^*	−147.8836	42.6
diazirine–diazomethane T_1 transition state (Figure 6e)	^3n–π^*	−147.7929	99.5
diazomethane $T_1 \rightarrow N_2 + {}^3CH_2$ transition state (Figure 6f)	^3n–π^*	−147.8889	39.3
diazirine $T(^3\pi$–$\pi^*)/T(^3n$–$\pi)$ intersection C_{2v} (Figure 6g)	$^3\pi$–$\pi^*/^3n$–π^*	−147.771	113.6
diazirine T_1/S_0 intersection (Figure 6h)	$S_0/^3n$–σ^*	−147.870	51.1
diazirine $T(^3n$–$\sigma^*)/T(^3n$–$\pi)$ intersection C_1 (Figure 6i)	^3n–$\sigma^*/^3n$–π^*	−147.775	110.6
diazomethane T_1/S_0 intersection (Figure 6j)	$S_0/^3n$–π^*	−147.884	42.3

However, the rigorous location of funnels corresponding to low-lying conical intersection points[8,26,27] requires a nonstandard method[28] that has been implemented in a development version of the same package. This method has been used to optimize the conical intersection structures in several recent papers[29] and will not be discussed further. The nonadiabatic coupling (NAC) and gradient difference (GD) vectors define the branching space[26n] at the conical intersection point, along which the degeneracy is lifted. These vectors are computed as part of the optimization method, and their significance will be discussed further subsequently. For all the computations of surface crossings, state-averaged orbitals have been used. Consequently, the energies of the surface crossings are quoted to 0.001 E_h. In all cases, the difference in energy between the two states at a crossing was less than this. For a discussion of singlet–triplet crossings (see the recent general paper by Yarkony[30]), a similar approach has been used, as we shall subsequently discuss. The spin–orbit coupling matrix elements have been computed using the techniques recently described by Koseki et al.[31]

It is appropriate at this point to comment on the reliability and appropriateness of the methods used. MC-SCF methods are essential in this problem. Not only must one be able to describe bond breaking, but also one needs to describe ground and excited states in a balanced way. The active space is chosen so that the bonding between the CH_2 fragment and the N_2 fragment in ground and excited states can be described for all possible orientations of the two fragments. SCF methods are clearly inappropriate. In a series of "benchmark" computations, Roos and coworkers[32] have calibrated the efficiency of MC-SCF methods in the very detailed computation of vertical excitation energies in hydrocarbons. It has also been established in ground-state multibond reactivity problems that MC-SCF methods are capable of reproducing the correct surface topology (minima, transition states, etc.); however, accurate energies (barrier heights, etc.) require some treatment of dynamic electron correlation. The *mechanism* of a reaction is specified by the number and nature of various topological features on the potential energy surface and the reaction paths that interconnect them. Thus, to answer mechanistic questions, MC-SCF can be adequate. With the active space and basis set used in this work, the singlet–triplet splitting at the triplet equilibrium geometry is computed as 9.26 kcal mol^{-1}, with the accepted value of 8.5 kcal mol^{-1}. For comparison with kinetic information, accurate energies and a treatment of dynamic correlation are required. Our objective in this paper is to suggest possible mechanistic rationalization of the sophisticated experimental data related to carbene formation from diazirines. As we shall discuss, the existence of conical intersections and singlet–triplet crossings turns out to be the central mechanistic feature. The existence of these topological features is a fundamental property of the electronic nature of the states involved and will survive a more accurate treatment of dynamic correlation. Further, the existence of minima and certain reaction paths provides the key to the understanding of the experimental data. More accurate energetics become important at a later stage if one is to interpret subtle dynamic effects.

Results and Discussion

In this section we shall document the main features of the singlet and triplet excited-state surfaces associated with the adiabatic deformation of diazirine and diazomethane and the subsequent internal conversion to diazoalkane isomers. For diazirine we will also describe the pathway for the formation of an excited-state diradical followed by internal conversion and production of singlet carbene with N_2 extrusion. A triplet pathway for the production of N_2 and triplet carbene via S_1/T_1 intersystem crossing has also been documented below. The energetic data for all the optimized geometries are collected in Table 1. The

(26) (a) Bonacic-Koutecky, V.; Koutecky, J.; Michl, J. *Angew. Chem., Int. Ed. Engl.* **1987**, *26*, 170. (b) Von Neunann, J.; Wigner, E. *Physik. Z.* **1929**, *30*, 467. (c) Teller, E. *J. Phys. Chem.* **1937**, *41*, 109. (d) Herzberg, G.; Longuet-Higgins, H. C. *Trans. Faraday Soc.* **1963**, *35*, 77. (e) Herzberg, G. *The Electronic Spectra of Polyatomic Molecules*; Von Nostrand: Princeton, 1966; p 442. (f) Mead, C. A.; Truhlar, D. G. *J. Chem. Phys.* **1979**, *70*, 2284. (g) Mead, C. A. *Chem. Phys.* **1980**, *49*, 23. (h) Keating, S. P.; Mead, C. A. *J. Chem. Phys.* **1985**, *82*, 5102. (i) Keating, S. P.; Mead, C. A. *J. Chem. Phys.* **1987**, *86*, 2152. (j) Davidson, R. E.; Borden, W. T.; Smith, J. *J. Am. Chem. Soc.* **1978**, *100*, 3299. (k) Mead, C. A. The Born-Oppenheimer approximation in molecular quantum mechanics. In *Mathematical frontiers in computational chemical physics*; Truhlar, D. G., Ed.; Springer: New York, 1987; Chapter 1, pp 1–17. (l) Bernardi, F.; De, S.; Olivucci, M.; Robb, M. A. *J. Am. Chem. Soc.* **1990**, *112*, 1737–1744. (m) Bernardi, F.; Olivucci, M.; Robb, M. A. *Acc. Chem. Res.* **1990**, *23*, 405–412. (n) Atchity, G. J.; Xantheas, S. S.; and Ruegenberg, K. *J. Chem. Phys.* **1991**, *95*, 1862.

(27) Salem, L. *Electrons in Chemical Reactions: First Principles*; Wiley: New York, 1982.

(28) Ragazos, I. N.; Robb, M. A.; Bernardi, F.; Olivucci, M. *Chem. Phys. Lett.* **1992**, *197*, 217.

(29) (a) Bernardi, F.; Olivucci, M.; Ragazos, I. N.; Robb, M. A. *J. Am. Chem. Soc.* **1992**, *114*, 2752–2754. (b) Bernardi, F.; Olivucci, M.; Robb, M. A.; Tonachini, G. *J. Am. Chem. Soc.* **1992**, *114*, 5805–5812. (c) Bernardi, F.; Olivucci, M.; Ragazos, I. N.; Robb, M. A. *J. Am. Chem. Soc.* **1992**, *114*, 8211–8220. (d) Palmer, I.; Bernardi, F.; Olivucci, M.; Robb, M. A. *J. Org. Chem.* **1992**, *57*, 5081–5087. (e) Palmer, I.; Ragazos, I. N.; Bernardi, F.; Olivucci, M.; Robb, M. A. *J. Am. Chem. Soc.* **1992**, *115*, 673–682. (f) Reguero, M.; Bernardi, F.; Jones, H.; Olivucci, M.; Robb, M. A. *J. Am. Chem. Soc.* **1993**, *115*, 2073–2074. (g) Olivucci, M.; Ragazos, I. N.; Bernardi, F.; Robb, M. A. *J. Am. Chem. Soc.* **1993**, *115*, 3710–3721.

(30) Yarkony, D. R. *J. Am. Chem. Soc.* **1992**, *114*, 5406–5411.

(31) Koseki, S.; Schmidt, M. W.; Gordon, M. S. *J. Phys. Chem.* **1992**, *96*, 10768–10772.

(32) (a) Serranoandres, L.; Merchan, M.; Nebotgil, I.; Lindh, R.; Roos, B. O. *J. Chem. Phys.* **1993**, *98*, 3151–3162. (b) Roos, B. O.; Andersson, K.; Fulscher, M. P. *Chem. Phys. Lett.* **1992**, *192*, 5–13.

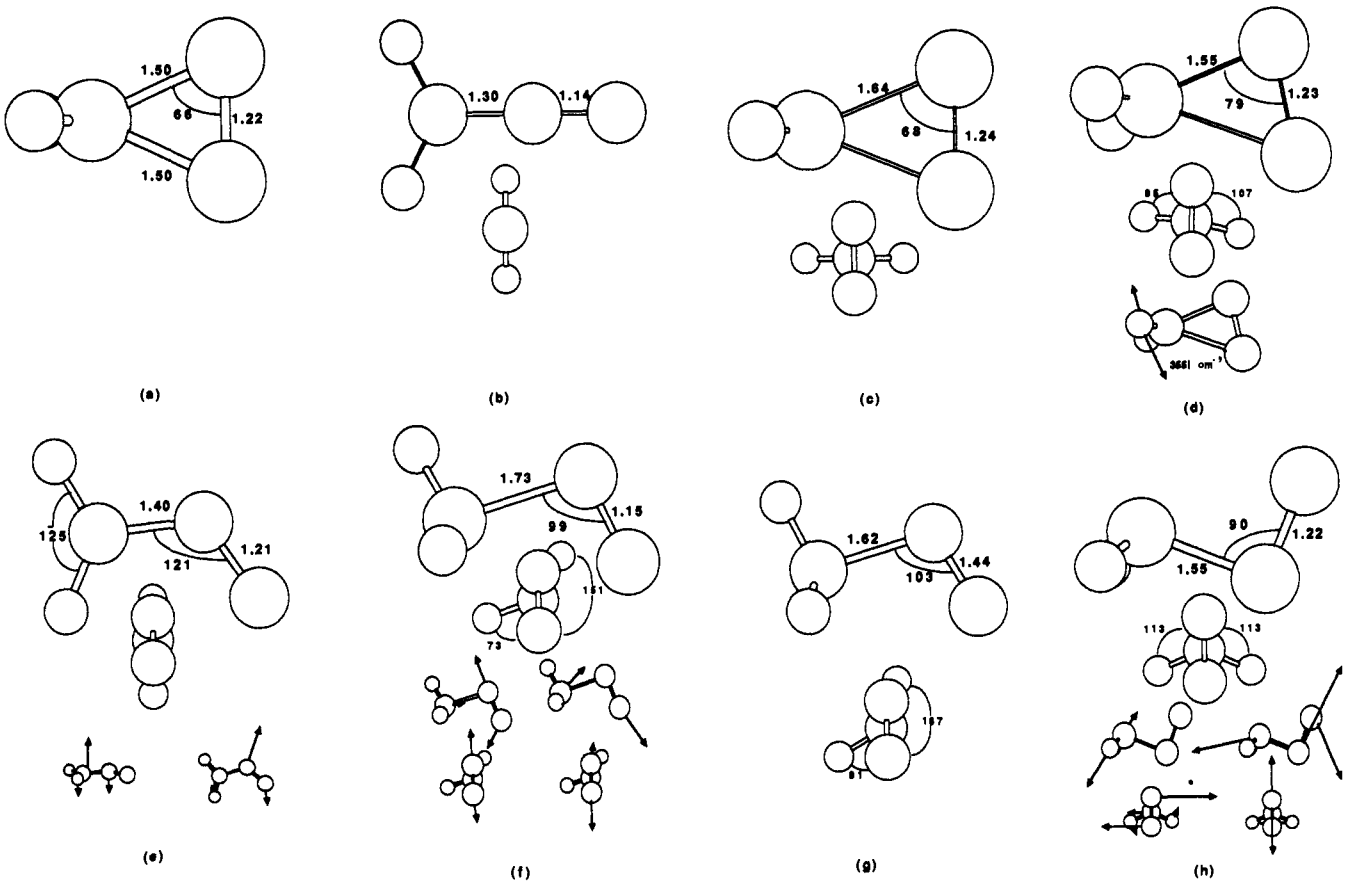

Figure 1. Optimized structures on S_0 and S_1 surfaces: (a) ground-state diazirine; (b) ground-state diazomethane; (c) diazirine S_1 minimum (^1n–π^*); (d) diazirine–diazomethane S_1 transition state (^1n–π^*); (e) diazomethane S_0/S (^1n–π^*) $^1D_{\sigma\pi}$ conical intersection, the two drawings at the bottom of the figure correspond to the directions of the nonadiabatic coupling (left) and gradient difference (right); (f) diradical ^1n–σ^*/S_0 conical intersection ($^1D_{\sigma\sigma}$, see Chart 3c), the nonadiabatic coupling (left) and gradient difference (right) are shown as in e; (g) diradical–diazomethane transition state (^1n–$\sigma^*/^1n$–π^* avoided crossing); (h) diazirine ^1n–$\sigma^*/^1n$–π^* conical intersection (C_{2v}) symmetry, the nonadiabatic coupling (left) and gradient difference (right) are shown as in e.

optimized structures can be found in Figures 1 and 6.

(i) $^1D_{\sigma\pi}$ Reaction Path for Adiabatic Rearrangement of Diazirine with Internal Conversion to Diazomethane. The optimized structures for ground-state diazirine and diazomethane are given in Figure 1a and b. The vertical excitation energies are collected in Table 1. The optimized geometries for ground-state diazirine and diazomethane are in good agreement with the MP2/6-31G* values of Boldyrev et al.[33] and the experimental values quoted therein. For example, the computed N–N distances in diazirine and diazomethane are 1.22 and 1.14 Å, respectively, which compares with the experimental values of 1.23 and 1.14 Å. The S_1 diazirine (Figure 1c) lies in a very shallow minimum, just 7 kcal mol^{-1} lower in energy than the Franck–Condon excitation (the lowest frequency normal mode is 134 cm^{-1} and corresponds to twist of the CH_2 group). At less than 0.5 kcal mol^{-1} above this minimum, there is a transition state (Figure 1d) that lies on an essentially **bop**-C_1 path between the S_1 diazirine minimum and diazomethane. The normal coordinate corresponding to the imaginary frequency 335i cm^{-1} involves rotation of the N_2 moiety. An IRC from this transition state (Figure 2) follows a **bop**-C_1 reaction path and terminates at a S_0/S_1 diradicaloid ($^1D_{\sigma\pi}$) conical intersection (the lowest energy point on this conical intersection is shown in Figure 1e). Restarting the IRC on the ground state leads simply (via a **bip** path) to diazomethane, as shown in Figure 2.

The directions of the nonadiabatic coupling (NAC) and gradient difference (GD) vectors for the diazomethane S_0/S_1 (^1n–π^*) $^1D_{\sigma\pi}$ conical intersection are plotted in Figure 1e and define a plane in the space of nuclear motions. Motion in this plane (the branching space) lifts the degeneracy, while the energy has been minimized in the remaining ($n-2$)-dimensional space Chart 4. These two special directions correspond to bending in-plane (GD) and bending out-of-plane (NAC). In this case, the S_1 (^1n–π^*) state (Chart 2c) has symmetry A'', while S_0 has symmetry A' in C_s. Thus, the GD is totally symmetric, while the NAC is nontotally symmetric. In fact, this structure corresponds to the global minimum of the diazirine/diazomethane n–π^* excited-state surface. However, while the energy is minimized, the $^1D_{\sigma\pi}$ structure shown in Figure 1e is a conical intersection rather than a true minimum as the energy gradient does not go to zero. Further, an IRC beginning at the diazomethane S_1 (^1n–π^*) Franck–Condon region terminates at this conical intersection (Figure 1e), as shown in Figure 3. Thus, photoexcitation of diazoalkanes gives rise to the same decay path as photoexcitation of diazirines. The energy of the conical intersection lies 36 kcal mol^{-1} above the $^1CH_2 + N_2$ product reference. Thus, depending on the rate of loss of energy to the surroundings and to internal vibrational modes, this path could ultimately lead to carbene as well.

To conclude this section, we need to comment on the possibility of the production of excited $^1CH_2$ ($^1B_1$), which has been postulated[21-24] to explain the higher reactivity of photochemically generated carbene with respect to thermally generated carbene. We have optimized the lowest energy point on the conical intersection that occurs between the $^1B_1$ and $^1A_1$ states in CH_2 itself. This occurs at a H–C–H angle of 140.5° and lies 28 kcal mol^{-1} above the energy of the optimum geometry of the $^1A_1$ state of $CH_2 + N_2$ and 4 kcal mol^{-1} below the $^1D_{\sigma\pi}$ conical intersection.

(33) Boldyrev, A. I.; Schleyer, P. v. R.; Higgins, D.; Thompson, C.; Kramarenko, S. S. *J. Comput. Chem.* **1992**, *13*, 1066–1078.

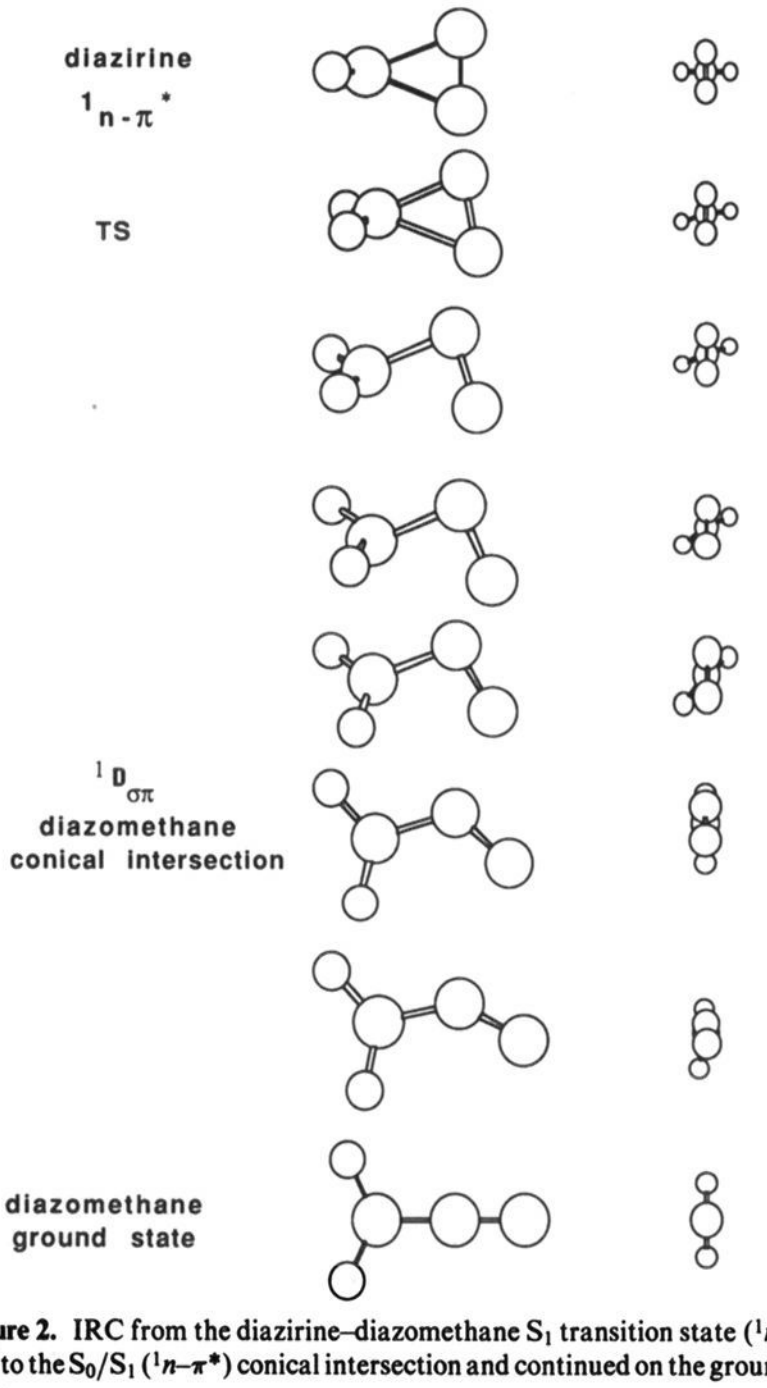

Figure 2. IRC from the diazirine–diazomethane S_1 transition state (^1n–π^*) to the S_0/S_1 (^1n–π^*) conical intersection and continued on the ground state.

Chart 4

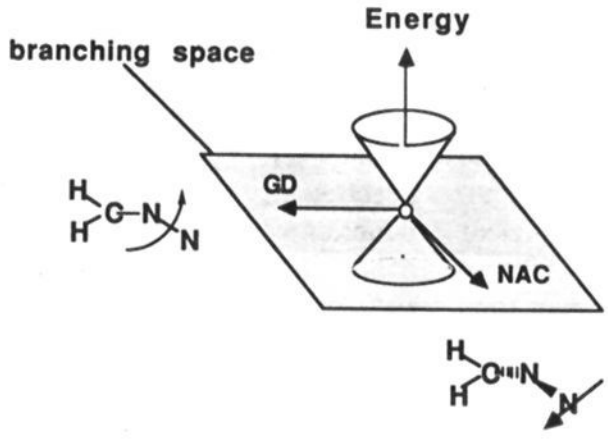

In fact, both of these points lie on the same conical intersection. A conical intersection is an $(n-2)$-dimensional hyperline. Various critical points will exist in this $(n-2)$-dimensional space, and we have simply found two minima. We could also find transition states within this $(n-2)$-dimensional space, but our programs have not been developed for this purpose yet. Extensive searches have shown that our conical intersection optimization methods always converged either to the $^1D_{\sigma\pi}$ conical intersection or the S_1/S_0 conical intersection in $^1CH_2 + N_2$. Thus, in principle, the system could decay anywhere along this $(n-2)$-dimensional hyperline, and the production of $^1B_1$ $CH_2 + N_2$ becomes possible. However, this is unlikely because there is a well-defined reaction path, shown in Figure 2, that will channel the system toward the $^1D_{\sigma\pi}$ diazomethane conical intersection exclusively.

(ii) $^1D_{\sigma\sigma}$ Reaction Path for Direct Production of Singlet Carbene with N_2 Extrusion. Based upon our introductory remarks, a **bop-**

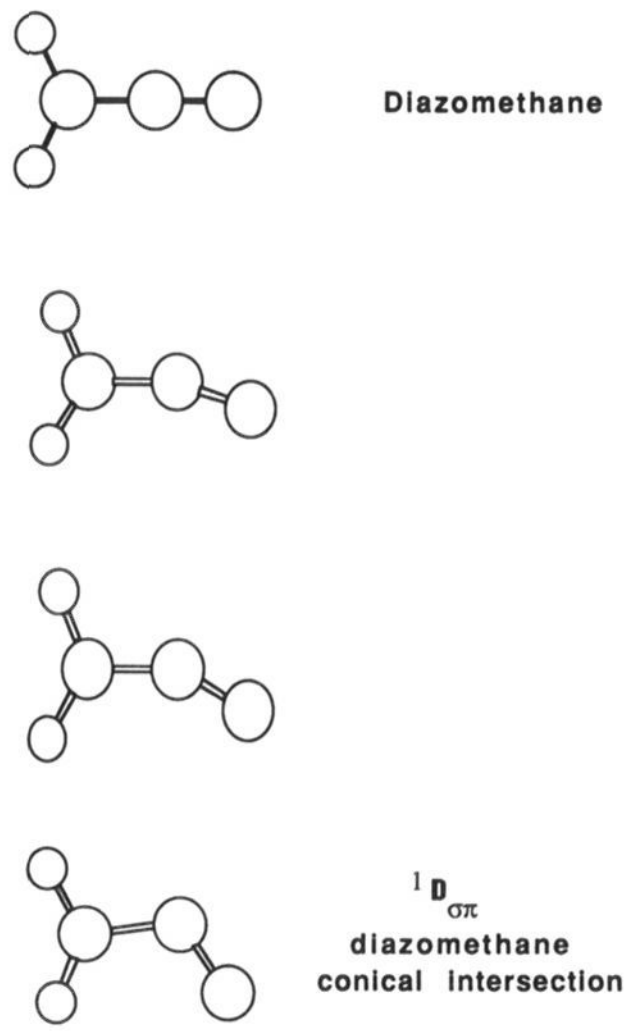

Figure 3. IRC (**bip**) from the diazomethane S_1 (^1n–π^*) Franck–Condon region to the S_0/S_1 (^1n–π^*) $^1D_{\sigma\pi}$ conical intersection.

C_1 excited-state reaction path ought to exist connecting diazirine to a $^1D_{\sigma\sigma}$ structure of the form shown in Chart 3c. A $^1D_{\sigma\sigma}$ structure corresponding to that shown in Chart 3c does indeed exist. In fact, this structure (Figure 1f) lies on a **bop-C_1** path from diazirine and has C_1 symmetry. It is not a true local minimum at all but is again the lowest energy point of a S_0/S_1 conical intersection. This structure lies 60 kcal mol^{-1} above $^1CH_2 + N_2$ and 48.8 kcal mol^{-1} below the Franck–Condon region. The nature of the potential energy surface in the region of this $^1D_{\sigma\sigma}$ conical intersection structure is rather subtle. All attempts to find a minimum on the diazirine-like surface (different from that shown in Figure 1c) always converged on the diazomethane $^1D_{\sigma\pi}$ conical intersection (Figure 1e). A scan along a (**bop-C_1**) *line* between the $^1D_{\sigma\sigma}$ diradical conical intersection (Figure 1f) and the diazirine minimum (Figure 1c) yields an energy profile with a slight maximum 4 kcal mol^{-1} above the diazirine S_1 minimum. This yields an upper bound to the barrier for decay via this path. However, a transition state could not be optimized in this region in spite of exhaustive attempts (computing analytical frequencies at every iteration). The only transition state that exists in this region is shown in Figure 1g and lies 3.7 kcal mol^{-1} above the $^1D_{\sigma\sigma}$ conical intersection (Figure 1f) and 38 kcal mol^{-1} below the diazirine–diazomethane S_1 transition state. Thus, the reaction path connecting the diazirine S_1 minimum and the diazomethane $^1D_{\sigma\pi}$ conical intersection (Figure 1e) must bifurcate with one branch, leading to the $^1D_{\sigma\sigma}$ conical intersection (Figure 1f). This conjecture is rather difficult to prove. However, some convincing evidence is presented in Figure 4, where we show the potential energy surface computed on a grid that contains the $^1D_{\sigma\sigma}$ conical intersection, the $^1D_{\sigma\pi}$ conical intersection, the $^1D_{\sigma\sigma}/^1D_{\sigma\pi}$ transition state, and the diazirine minimum. The curvature of the contour lines shows a bifurcation point indicated as an inset in Figure 4. The stream of arrows indicates the IRC (Figure 2) leading to the $^1D_{\sigma\pi}$ conical intersection. The broken line indicates a possible path leading to the $^1D_{\sigma\sigma}$ conical intersection via the bifurcation point. However, this is not a real reaction path. Rather, the valley leading to the $^1D_{\sigma\sigma}$ conical intersection will become populated from "vibrational leakage" (mainly rotation about the C–N bond) from the real reaction path that leads to the $^1D_{\sigma\pi}$

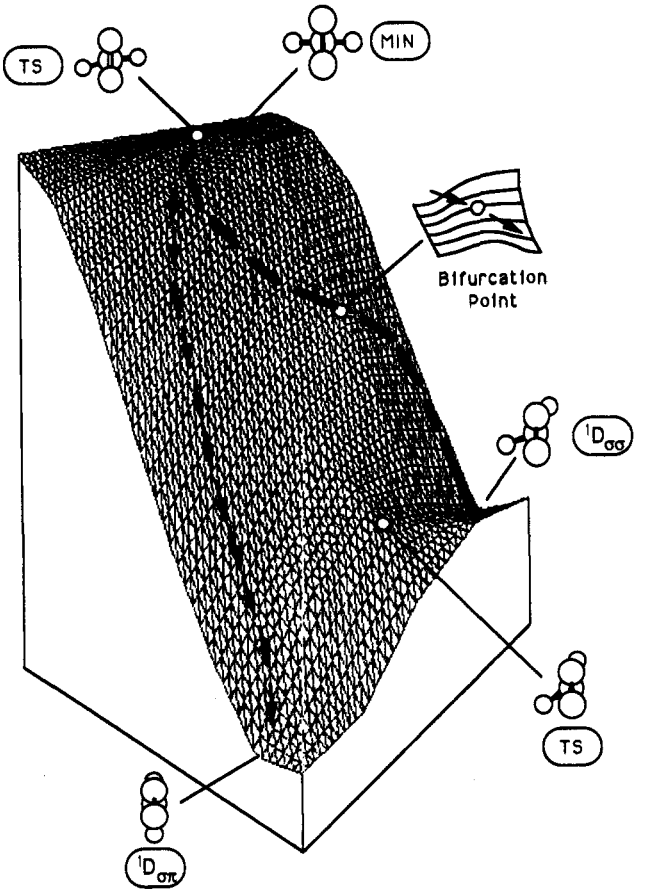

Figure 4. Potential energy surface computed on a grid that contains the $^1D_{\sigma\sigma}$ conical intersection, the $^1D_{\sigma\pi}$ conical intersection, the $^1D_{\sigma\sigma}/^1D_{\sigma\pi}$ transition state, and the diazirine minimum/transition state. Points were computed on a three-dimensional grid that involved the CH_2 out-of-plane bend, the C–N–N angle, and the H_2C–N_2 torsion. The two-dimensional grid plotted corresponds to a "cutting plane" containing the diazirine minimum and the $^1D_{\sigma\sigma}/^1D_{\sigma\pi}$ conical intersections. Thus the axes shown correspond to linear combinations of the original three grid variables.

conical intersection. Finally, an IRC beginning on the ground-state surface at the $^1D_{\sigma\sigma}$ conical intersection (Figure 1f) terminates at the products $^1CH_2 + N_2$ and is shown in Figure 5.

Since the proposed pathway involving a reaction path for direct production of singlet carbene with N_2 extrusion via $^1D_{\sigma\sigma}$ is rather novel, we need to discuss some additional evidence. The reaction path for the adiabatic rearrangement of diazirine with internal conversion to diazomethane involves the n–π^* state. However, since S_1 diazirine corresponds to an n–π^* state while the $^1D_{\sigma\sigma}$ diradical is an n–σ^* state, we expect to be able to find an avoided crossing and a transition state. In C_{2v} symmetry, the n–σ^* and n–π^* states have different symmetry, and the crossing only becomes avoided as the symmetry is lifted by rotation about the C–N bond. Thus, one can search for the S_1/S_2 conical intersection between the n–σ^* and n–π^* states in C_{2v} symmetry, and the resulting structure (12 kcal mol^{-1} above S_1 diazirine) is shown in Figure 1h. The gradient difference vector shown in Figure 1h (that must be totally symmetric) involves mainly the C–N–N angle bend, while the nonadiabatic coupling vector (that must be nontotally symmetric) involves mainly rotation about the C–N bond. Movement in this plane lifts the degeneracy, and the avoided crossing transition state (if it exists) must lie at some finite distortion along the nontotally symmetric, nonadiabatic coupling vector. In fact, as we have discussed, such an n–π^*/n–σ^* transition state does exist (Figure 1g); however, as shown in Figure 4, it connects the diazomethane $^1D_{\sigma\pi}$ conical intersection (Figure 1e) and the $^1D_{\sigma\sigma}$ conical intersection (Figure 1f).

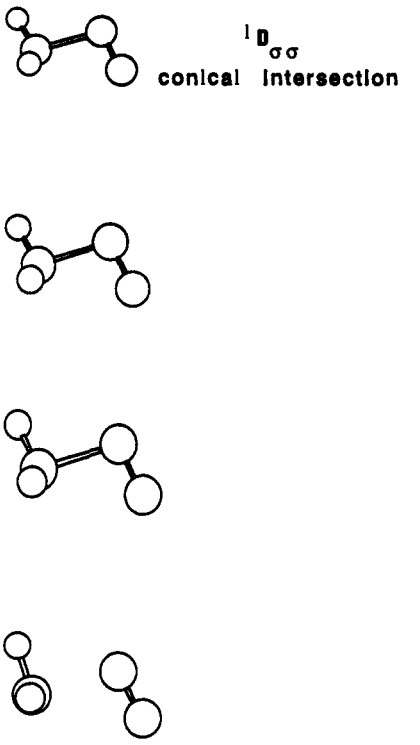

Figure 5. IRC from the $^1D_{\sigma\sigma}$ ^1n–σ^*/S_0 conical intersection to N_2 + $^1CH_2$.

In conclusion, the data above support the idea that only a small amount of n–π^* diazirine decays via the $^1D_{\sigma\sigma}$ conical intersection, generating $^1CH_2 + N_2$. The situation would be quite different for diazirines prepared in the n–σ^* excited state. Our computations suggest that there are two possible routes to n–σ^* diazirine. The first route is adiabatic and involves motion from the excited-state n–π^* minimum toward the region of the S_0/S_1 $^1D_{\sigma\sigma}$ point. Despite the fact that we have been unable to find a transition structure connecting these points, we have demonstrated that the barrier along a **bop-C_1** *line* cannot be larger then 4 kcal mol^{-1} (see above). Thus, depending on the actual barrier and relaxation dynamics, this path could actually compete with the path to the $^1D_{\sigma\pi}$ conical intersection, which involves a barrier of .55 kcal mol^{-1}. The second route involves excitation to S_2 and fast decay to S_1. In this case, the photoexcited diazirine would decay via a S_1/S_2 C_{2v} conical intersection directly to the S_0/S_1 $^1D_{\sigma\sigma}$ point, leading to efficient production of $^1CH_2 + N_2$ and almost no production of diazomethane. This suggests a possible wavelength dependence of the photochemistry of diazirines.

(iii) Reaction Paths for Production of a Triplet Carbene. We now turn our attention to the triplet surfaces and the crossing points with S_0 and with S_1. Since the surface topology is rather complicated, we will unify our discussion by using Chart 5, which shows a simplified representation of the important topological features and relative energetics. In Chart 5, we show two cross sections along **bop-C_s** and **bip** coordinates. The contours at the bottom of the diagram are intended to indicate the main topological features of the lowest triplet surface (i.e., T_1). The various optimized structures on the diazirine–diazomethane triplet surface are collected in Figure 6, and the energetics are summarized in Table 1.

The triplet diazirine–diazomethane surface is complicated by the fact that there are three low-lying triplet states in the Franck–Condon region. One has the ^3n–π^* and ^3n–σ^* states which behave in a similar manner to the corresponding singlets. However, for diazirine itself, the lowest energy triplet is the $^3\pi$–π^* state, where the excitation is localized on N_2, and we will have an elongated N_2 bond (optimized geometry in Figure 6b). We begin with a discussion of the behavior of the triplet manifold in the **bop-C_s**

Chart 5

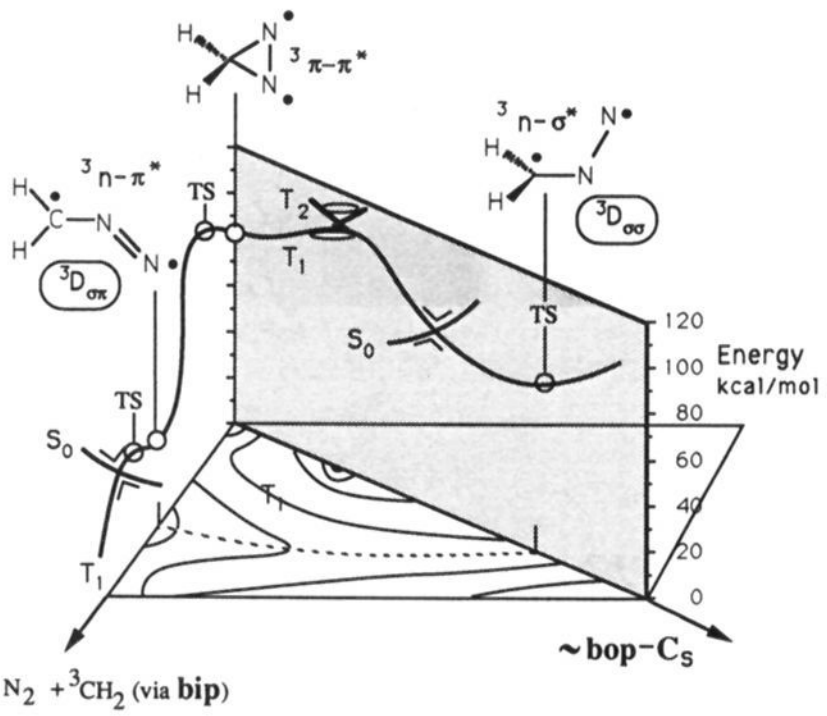

plane in Chart 5. As the C–N–N angle opens along a **bop-C_s** path, the energy of the $^3\pi-\pi^*$ state rises rapidly and the energies of the $^3n-\pi^*$ and $^3n-\sigma^*$ states decrease. At C–N–N angles between 60° and 80°, we have located crossing points (conical intersection geometries are given in Figure 6g and i) between these triplet states, either on or near the **bop-C_s** plane, and the T_1/T_2 $^3n-\pi^*/^3\pi-\pi^*$ conical intersection is indicated in Chart 5. As the C–N–N angle opens along a **bop-C_s** coordinate, the $^3n-\sigma^*$ state becomes strongly stabilized, while as one rotates the N_2 along a **bop-C_1** coordinate, the $^3n-\pi^*$ state becomes stabilized. Thus, for larger C–N–N angles, the $^3n-\sigma^*$ is the lowest energy triplet state along the **bop-C_s** coordinate, and the $^3n-\pi^*$ is the lowest energy triplet state along the **bip** coordinate.

At a C–N–N angle of 116°, along a **bop-C_s** coordinate, the $^3n-\sigma^*$ state becomes the lowest energy triplet state, and we have located a $^3D_{\sigma\sigma}$ critical point (optimized geometry in Figure 6d) that is, in fact, a transition state ($250i$ cm^{-1}) between two bent, in-plane diazomethane $^3D_{\sigma\pi}$ minima (optimized geometry in Figure 6c) that are shown in the **bip** plane in Chart 5. The lowest energy path between diazirine and the bent, in-plane diazomethane $^3D_{\sigma\pi}$ minimum involves a **bop-C_1** coordinate that lies between the two planes shown in Chart 5. Along this coordinate, there will be an avoided crossing between the $^3\pi-\pi^*$ and $^3n-\pi^*$ states and thus a transition state (barrier from the $^3\pi-\pi^*$ diazirine is 9 kcal mol^{-1}) for the isomerization to diazomethane that lies on the $^3n-\pi^*$ surface. This transition state is shown as TS in Chart 5 on the **bip** plane for clarity, although the true TS lies about midway between the two planes, as shown by the optimized geometry in Figure 6e. The low-energy N_2 extrusion channel from the diazomethane $^3D_{\sigma\pi}$ minimum lies along a **bip** coordinate with a 7 kcal mol^{-1} barrier (optimized transition-state geometry in Figure 6f). From a theoretical point of view, it is interesting to note that bent $^3D_{\sigma\pi}$ diazomethane has a true existence on the triplet surface but the $^1D_{\sigma\pi}$ point is the minimum of a conical intersection on the singlet surface. Further, the diradical $^{1,3}D_{\sigma\sigma}$ structure proposed in Chart 3c exists as a real critical point on the triplet surface (a transition state) and as a conical intersection on the singlet surface.

Thus, direct excitation into the triplet manifold leads either to a triplet $^3\pi-\pi^*$ diazirine minimum with a small barrier to isomerization to triplet bent diazomethane or to a higher energy $^3n-\pi^*$ state which can lead, via the T_1/T_2 conical intersection, to diazirine or triplet $^3D_{\sigma\pi}$ diazomethane via the $^3D_{\sigma\sigma}$ TS. Production of $^3CH_2 + N_2$ then results over a 7 kcal mol^{-1} barrier.

The S_0 surface cuts the triplet surface near the extrusion path in the **bip** plane (optimized geometry in Figure 6j) and near the $^3D_{\sigma\sigma}$ critical point in the **bop-C_s** plane (Figure 6h). At a C–N–N angle of 98° on a **bop-C_1** coordinate, there is a point where one has a $T_2(^3n-\pi^*)/S_1(^1n-\pi^*)$ crossing minimum (optimized geometry in Figure 6a) which provides the point where intersystem crossing from singlet to triplet can occur, and we shall discuss this feature in more detail subsequently. Near this point, the $T_1(^3n-\sigma^*)/S_0$ crossing minimum also occurs (Figure 6h). The approximate location of this point is also shown in the **bop-C_s** plane in Chart 5. Finally, for completeness, we have also optimized the geometry of the $^1CH_2$ ($^1A_1$) and $^3CH_2$ ($^1B_1$) crossing. The crossing occurs with an H–C–H angle of 93.8° and lies 22 kcal mol^{-1} above $^3CH_2$ ($^1B_1$) and 7.8 kcal mol^{-1} above $^1CH_2$ ($^1A_1$).

The intersystem crossing decay path from S_1 involves low-energy points where singlet and triplet states are degenerate. In fact, the vertical excitation energies (Table 1) for $^3n-\pi^*$, $^3\pi-\pi^*$, and $^1n-\pi^*$ are similar and differ by 12 kcal mol^{-1}. The lowest energy point of the $S_1(^1n-\pi^*)/T_2(^3n-\pi^*)$ crossing occurs along a **bop-C_1** path at a geometry (shown in Figure 6a) some 3.5 kcal mol^{-1} below the diazirine–diazomethane S_1 ($^1n-\pi^*$) transition state. Notice that the geometry of the crossing point (Figure 6a) is similar to that of the diazirine–diazomethane S_1 ($^1n-\pi^*$) transition state (Figure 1d).

The probability P of the intersystem crossing has recently been discussed by Yarkony[30] and depends on the magnitude of the spin–orbit coupling matrix element H_{IJ}^{SO}, on the difference in gradient of the singlet and triplet states g_{IJ} (a small gradient difference gives rise to an efficient crossing), and on the velocity v as shown in eq 1.

$$P = 1 - \exp\left[-\frac{\pi}{4}\left(\frac{8|H_{IJ}^{SO}|^2}{g_{IJ}v}\right)\right] \qquad (1)$$

In the present case, the gradients of ($^1n-\pi^*$) and ($^3n-\pi^*$) states are similar, as expected, and the efficiency of intersystem crossing would be predicted to be high. Further, dynamically, the efficiency of intersystem crossing will depend upon the velocity v along a path through the singlet–triplet crossing: a low velocity will favor efficient crossing. Again, for a reaction path on S_1, the velocity will be low because we are near a transition state, and this will favor efficient intersystem crossing. The gradient difference vector is also shown in Figure 6a. This is the direction that corresponds to motion from the singlet to the triplet surface; notice it is almost parallel to the direction of negative curvature in the S_1 transition state shown in Figure 1d. The spin–orbit coupling H_{IJ}^{SO} was computed (in a one-electron approximation using the effective charges of N = 4.55 and C = 3.6 optimized by Koseki et al.[31]) at the lowest energy crossing point. The result is very small: H_{IJ}^{SO} = 3.98 cm^{-1}. Thus, for this unsubstituted system, while the intersystem crossing decay path is accessible, it will not be efficient. Thus, one would not expect to see products that arise via this route because the barrier to decay from the diazirine S_1 minimum via the $^1D_{\sigma\pi}$ diazomethane conical intersection or the $^1D_{\sigma\sigma}$ conical intersection is negligible, and this process will occur on a much faster time scale.

Conclusions

Our results indicate that the singlet photochemistry of diazirine and diazomethane is controlled by three efficient radiationless decay paths via two different S_0/S_1 conical intersections. We have characterized one competitive pathway (see Figure 4) for decay from a shallow $^1n-\pi^*$ diazirine minimum via a bent, in-plane diazomethane-like $^1D_{\sigma\pi}$ conical intersection to ground-state diazomethane. Along this route, small quantities of $^1CH_2 + N_2$ may get formed via vibrational leaking to a diradicaloid $^1D_{\sigma\sigma}$ conical intersection. A second efficient route leading to direct photoproduction of $^1CH_2 + N_2$ needs photoexcitation or conversion to the $n-\sigma^*$ state of diazirine and proceeds via final passage through the same $^1D_{\sigma\sigma}$ conical intersection. A third reaction path (Figure

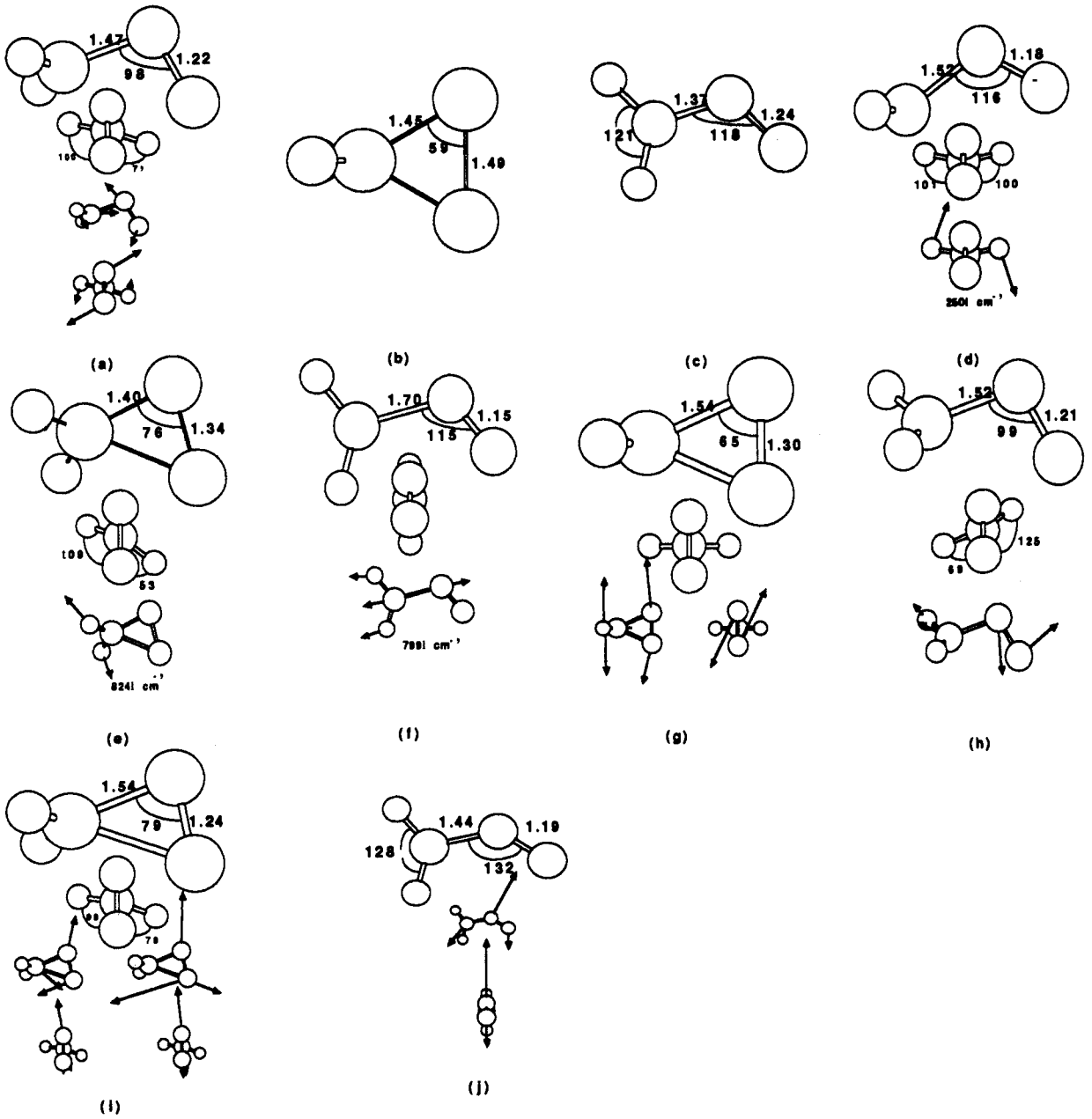

Figure 6. Optimized structures on triplet surfaces: (a) diazirine $T_2(^3n\text{–}\pi^*)/S_1(^1n\text{–}\pi^*)$ intersection, the direction of the gradient difference vector is indicated at bottom of the figure; (b) diazirine $T_1(^3\pi\text{–}\pi^*)$ minimum; (c) diazomethane $T_1(^3n\text{–}\pi^*)$ $^3D_{\sigma\pi}$ minimum; (d) $T_1(^3n\text{–}\sigma^*)$ $^3D_{\sigma\sigma}$ diazomethane critical point, a CN rotational transition state between two equivalent $^3D_{\sigma\pi}$ diazomethane minima; (e) diazirine–diazomethane $T_1(^3n\text{–}\pi^*)$ transition state; (f) diazomethane $^3D_{\sigma\pi}$ $T_1(^3n\text{–}\pi^*) \rightarrow N_2 + {}^3CH_2$ transition state; (g) C_{2v} diazirine T_1/T_2 intersection ($^3\pi\text{–}\pi^*/^3n\text{–}\pi^*$), the two drawings at the bottom of the figure correspond to the directions of the nonadiabatic coupling (left) and gradient difference (right); (h) diazirine $T_1(^3n\text{–}\sigma^*)/S_0$ intersection, the direction of the gradient difference vector is shown at the bottom of the figure; (i) diazirine T_1/T_2 intersection ($^3n\text{–}\pi^*/^3n\text{–}\sigma^*$), the nonadiabatic coupling and the gradient difference vectors are shown as in g; (j) diazomethane $T_1(^3n\text{–}\pi^*)/S_0$ intersection, the direction of the gradient difference vector is shown at the bottom of the figure.

3) exists from the Franck–Condon region of diazomethane to the $^1D_{\sigma\pi}$ conical intersection that can also lead to $^1CH_2 + N_2$ on the ground-state surface.

The triplet path (Chart 5) is similar to the singlet and begins at a $^3\pi\text{–}\pi^*$ minimum, passing over a transition state to an $^3n\text{–}\pi^*$ $^3D_{\sigma\pi}$ bent diazomethane minimum and then over another transition state to $^3CH_2 + N_2$. The lowest energy point for singlet (S_1)-to-triplet intersystem crossing (i.e., $^{1,3}n\text{–}\pi^*$ crossing) occurs at a geometry that is similar to the transition state between the $^1n\text{–}\pi^*$ diazirine minimum and the bent, in-plane diazomethane-like $^1D_{\sigma\pi}$ conical intersection. However, the efficiency of the intersystem crossing is predicted to be very low, and since the barriers for the singlet decay processes are negligible, the singlet decay process will occur on a shorter time scale.

The nature of the $D_{\sigma\pi}$ and $D_{\sigma\sigma}$ diradicaloids first suggested by Devaquet[10] is now established. A bent, in-plane, excited-state $^{1,3}D_{\sigma\pi}$ diazomethane-like structure exists as a true minimum on the triplet surface and as the lowest energy point on a conical intersection on the singlet surface. Similarly, a ring-opened diradicaloid form $^{1,3}D_{\sigma\sigma}$ of diazirine exists as a transition state on the triplet surface and as a conical intersection on the singlet surface.

Our results support a unified mechanistic picture for singlet diazirine and diazomethane photochemistry that is consistent with modern experimental results. This mechanistic picture is based upon the existence of excited-state reaction paths passing through conical intersections where a fully efficient return to the ground state is possible. The implicit assumption is that the

Chart 6

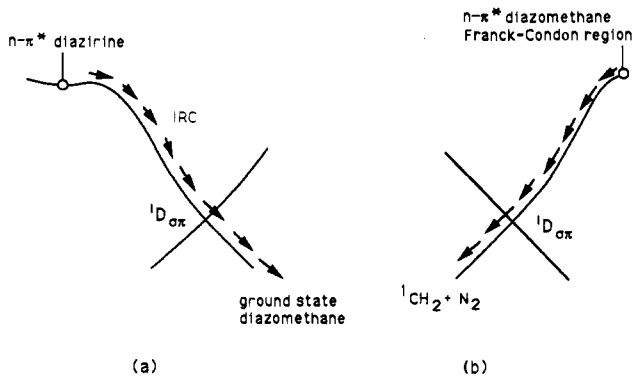

direction of the momentum along the excited-state IRC will be essentially unchanged on the ground-state surface after decay from the conical intersection. We now summarize the central mechanistic implications.

The temperature dependence of the fluorescence intensity of 3,3-dialkyldiazirines[5] is consistent with the existence of a shallow minimum on the excited state of diazirine, which is separated from a fast radiationless decay region by a 0.02–1.5 kcal mol^{-1} barrier. Our results show that an excited-state diazirine minimum does indeed exist on the n–π^* surface of diazirine. Further, the computed barrier on the path leading to the diazomethane-like $^1D_{\sigma\pi}$ conical intersection, where fast radiationless decay is possible, and then to ground-state diazomethane is 0.5 kcal mol^{-1}. The possible evolution of the n–π^* diazirine after decay through the $^1D_{\sigma\pi}$ conical intersection has been illustrated in Chart 6a (see the IRC in Figure 2). During the excited-state relaxation toward the $^1D_{\sigma\pi}$ point, the system accumulates kinetic energy along the geometrical coordinate, leading to diazomethane (IRC in Figure 2). Thus, after decay via the $^1D_{\sigma\pi}$ conical intersection, the direction of the momentum will be toward diazomethane so that the primary product of diazirine photolysis should be diazomethane in a highly excited vibrational state. From the excited-state part of the IRC shown in Figure 2, it is apparent that the momentum will be directed along C–N rotation, C–N–N angle-opening, and C–N compression (the C–N distance is 1.5 Å in diazirine, 1.4 Å at the $^1D_{\sigma\pi}$, and 1.3 Å in diazomethane). Thus, it is unlikely that the system will evolve from diazomethane to produce singlet carbene and N_2 by the diversion of the momentum along a ground-state N_2 extrusion pathway. Although the system will have accumulated sufficient kinetic energy during its decay motion (the $^1D_{\sigma\pi}$ conical intersection lies 73 kcal mol^{-1} below the Franck–Condon region), the momentum will be directed in rotation about the C–N bond, C–N–N bending, and CN compression. It is well known that this excess vibrational energy is rapidly dissipated in a 6 K matrix so that the system will equilibrate at the ground-state diazomethane structure. Thus, the observed efficient production of $CH_2 + N_2$ is unlikely to occur directly from n–π^* diazirine via the highly accessible $^1D_{\sigma\pi}$ path.

There are two alternative routes to N_2 extrusion from diazirines: (1) via the $^1D_{\sigma\sigma}$ conical intersection, leading directly to $N_2 + {}^1CH_2$ as shown in Figure 4 and (2) via a two-photon process (Chart 6b) involving secondary photoexcitation of the primary diazomethane product, leading to n–π^* excited diazomethane, which can then decay (see Figure 3) via the same $^1D_{\sigma\pi}$ conical intersection. Experimental results[1-6] indicate that carbenes are produced from diazirines via route 1 only. However, in the following we will describe both of these mechanistic possibilities.

Our computations on the first process indicate that decay via the $^1D_{\sigma\sigma}$ ^1n–σ^*/S_0 conical intersection leads directly to $N_2 + {}^1CH_2$ (see IRC in Figure 5). We have been unable to locate a transition state leading to this path from the ^1n–π^* diazirine minimum. A linear search gives an upper bound of 4 kcal mol^{-1} to the barrier. If the ^1n–π^* diazirine evolves exclusively via the **bop-C_1** transition state, then the $^1D_{\sigma\sigma}$ conical intersection can become populated only by vibrational leakage from the $^1D_{\sigma\pi}$ path. However, if the diazirine is converted or prepared to the n–σ^* excited state, then the $^1D_{\sigma\sigma}$ route becomes highly accessible, leading to efficient production of $N_2 + {}^1CH_2$. Thus, our computations support the proposal that the observed production of carbene from excited-state diazirine occurs from the n–σ^* excited state. In principle, this state can be reached via two different routes. The first involves deformation of n–π^* diazirine directly toward $^1D_{\sigma\sigma}$ by overcoming a small barrier. Despite the fact that we have not been able to locate a transition state leading to $^1D_{\sigma\sigma}$, we have found evidence that the barrier for this transformation must be lower than 4 kcal mol^{-1}. It is apparent that an evaluation of the dynamic factors would be required to determine whether this path may become more important than the $^1D_{\sigma\pi}$ path, which involves a barrier of only 0.55 kcal mol^{-1}. A second route involves initial promotion of diazirine to the n–σ^* excited state (S_2) followed by radiationless decay to S_1. This is possible via the passage through a S_1/S_2 conical intersection between the n–σ^* and n–π^* states. In this case, the diazomethane: $^1CH_2$ ratio may reflect the initial population of n–π^* and n–σ^* states. This ratio should also be sensitive to the irradiation wavelength.

The alternative two-photon process (photoexcitation of the primary diazomethane product) involves decay via the $^1D_{\sigma\pi}$ conical intersection, producing singlet carbene and N_2 plus a smaller amount of diazirine. While the reaction path (Figure 2 and Chart 6a) from n–π^* diazirine via the $^1D_{\sigma\pi}$ conical intersection leads to diazomethane, the reaction path (see Figure 3 and Chart 6b) from the Franck–Condon region of diazomethane to the $^1D_{\sigma\pi}$ conical intersection can lead directly to N_2 extrusion, as we shall now discuss. Along the IRC from the vertically excited diazomethane (Figure 3), the kinetic energy is accumulated in the bending of the C–N–N angle and the C–N stretch along a **bip** path. The C–N bond length stretches from 1.3 Å in the vertically excited diazomethane to 1.5 Å at the $^1D_{\sigma\pi}$ conical intersection. Since the motion will continue in the same direction after decay to the ground state, the system will continue to distort in such a way as to reduce the C–N–N angle and stretch the C–N bond, thus inducing a C–N bond-breaking process to produce N_2 in a highly excited rotational state. Diazirine cannot form along such a decay pathway since the system is planar. However, diversion from this type of motion along a nontotally symmetric **bop-C_1** coordinate could lead to a small amount of diazirine back-formation. This mechanism does not seem adequate for explaining carbene production from diazirines since diazomethane undergoes photoreaction at longer wavelength (400 nm) than diazirine (340 nm). Thus, during 340-nm photolysis, diazomethanes could only decompose with a very low quantum yield or possibly by exploiting diazirine fluorescence at 380–400 nm.[5] However, this same mechanism should be operative in diazoalkane photochemistry. Indeed, such a mechanism is consistent with recent matrix isolation photochemistry of diazoethane[1] and with older data on the production of carbenes via photolysis of diadamantylcarbene and di-*tert*-butylcarbene (see ref 4 and references therein).

According to our results for the triplet pathways, the production of $^3CH_2 + N_2$ must follow a very similar path to the singlet diazirine–diazomethane excited-state isomerization in the initial stage. Thus, population of the triplet state of diazirine will lead to N_2 extrusion + $^3CH_2$ via $^3D_{\sigma\pi}$ diazomethane with a barrier of 9 kcal mol^{-1}. However, the direct experimental study of this pathway is difficult. It is the intersystem crossing from the singlet to the triplet manifold that is the more interesting problem. Our results suggest that this intersystem crossing will not be efficient (very small spin–orbit coupling). Thus, because of negligible barriers on the singlet decay channels, the intersystem crossing

will not compete. This conclusion is supported by recent results obtained on 3,3-dimethyldiazirine[5] which suggest that the triplet state either is not formed on direct excitation or has a very short lifetime.

The mechanistic picture presented in this paper is based upon the existence of excited-state reaction paths passing through conical intersections, where a fully efficient return to the ground-state is possible. There should be little doubt that MC-SCF methods are capable of describing the surface topology correctly since these topological features are a fundamental property of the electronic structures of the states involved (see Charts 2 and 3). Thus, the mechanistic scheme should survive a more accurate treatment that includes dynamic electron correlation. The details of the energetics (e.g., the barrier to decomposition from singet–triplet diazirine) or the barrier that leads to the $^1D_{\sigma\sigma}$ would require a more accurate treatment.

Acknowledgment. This research has been supported in part by the SERC (U.K.) under Grants Numbers GR/G 03335 and GR/H94177. The authors are also grateful to IBM for support under a Joint Study Agreement. All computations were run on an IBM RS/6000. The authors also wich to thank Prof. Renzo Cimiraglia of the Dipartimento di Chimica, Universitá di Ferrara, Italy, who has kindly provided some of the computer routines used to evaluate the one-electron integrals for the spin–orbit coupling.